\$ SUPER

Contents lists available at ScienceDirect

Biomaterials Advances

journal homepage: www.journals.elsevier.com/materials-science-and-engineering-c





Characterizing properties of scaffolds 3D printed with peptide-polymer conjugates

Diana E. Hammerstone ^a, Tomas F. Babuska ^{b,c,1}, Santiago Lazarte ^d, Brandon A. Krick ^b, Lesley W. Chow ^{a,e,*}

- ^a Department of Materials Science and Engineering, Lehigh University, 5 E Packer Avenue, Bethlehem, PA 18015, USA
- b Department of Mechanical Engineering, FAMU-FSU College of Engineering, Florida State University, 2525 Pottsdamer Street, Building A Room A229, Tallahassee, FL 32310 USA
- ^c Department of Mechanical Engineering and Mechanics, Lehigh University, 19 Memorial Dr W, Bethlehem, PA 18015, USA
- ^d Department of Chemical and Biomedical Engineering, FAMU-FSU College of Engineering, Florida State University, 2525 Pottsdamer Street, Building A, Room A131, Tallahassee, FL 32310, USA
- ^e Department of Bioengineering, Lehigh University, 7 Asa Drive, Suite 205, Bethlehem, PA 18015, USA

ARTICLE INFO

Keywords:
3D printing
Biofabrication
Peptides
Biodegradable polymers
Surface functionalization
Scaffold mechanical properties

ABSTRACT

Three-dimensional (3D) printing is a popular biomaterials fabrication technique because it enables scaffold composition and architecture to be tuned for different applications. Modifying these properties can also alter mechanical properties, making it challenging to decouple biochemical and physical properties. In this study, inks containing peptide-poly(caprolactone) (PCL) conjugates were solvent-cast 3D printed to create peptidefunctionalized scaffolds. We characterized how different concentrations of hyaluronic acid-binding (HAbind-PCL) or mineralizing (E3-PCL) conjugates influenced properties of the resulting 3D-printed constructs. The peptide sequences CGGGRYPISRPRKR (HAbind-PCL; positively charged) and CGGGAAAEEE (E3-PCL; negatively charged) enabled us to evaluate how conjugate chemistry, charge, and concentration affected 3D-printed architecture, conjugate location, and mechanical properties. For both HAbind-PCL and E3-PCL, conjugate addition did not affect ink viscosity, filament diameter, scaffold architecture, or scaffold compressive modulus. Increasing conjugate concentration in the ink prior to printing correlated with an increase in peptide concentration on the scaffold surface. Interestingly, conjugate type affected final conjugate location within the 3D-printed filament cross-section. HAbind-PCL conjugates remained within the filament bulk while E3-PCL conjugates were located closer to the filament surface. E3-PCL at all concentrations did not affect mechanical properties, but an intermediate HAbind-PCL concentration resulted in a moderate decrease in filament tensile modulus. These data suggest final conjugate location within the filament bulk may influence mechanical properties. However, no significant differences were observed between PCL filaments printed without conjugates and filaments printed with higher HAbind-PCL concentrations. These results demonstrate that this 3D printing platform can be used to functionalize the surface without significant changes to the physical properties of the scaffold. The downstream potential of this strategy will enable decoupling of biochemical and physical properties to fine-tune cellular responses and support functional tissue regeneration.

1. Introduction

Biomaterial scaffolds for tissue engineering are designed to support the regeneration of lost or damaged tissues [1-4]. Three-dimensional (3D) printing has gained significant attention as a scaffold fabrication

technique because it offers key advantages, such as high spatial resolution, rapid production speed, and the ability to combine multiple materials and generate complex and patient-specific constructs [4–8]. Several types of 3D printing techniques have been used in biomaterials applications, including extrusion-based (i.e., fused deposition modeling

^{*} Corresponding author at: Department of Materials Science and Engineering, Lehigh University, 5 E Packer Avenue, Bethlehem, PA 18015, USA. E-mail addresses: deh220@lehigh.edu (D.E. Hammerstone), tfbabus@sandia.gov (T.F. Babuska), s.lazarte@fsu.edu (S. Lazarte), b.krick@famu.fsu.edu (B.A. Krick), lesley.chow@lehigh.edu (L.W. Chow).

¹ Sandia National Laboratories, 1515 Eubank Drive SE, Albuquerque, New Mexico 87123 USA.

(FDM) and direct ink writing), particle fusion-based (i.e., selective laser sintering), and light-assisted (i.e., stereolithography) approaches [5,6]. These techniques enable users to tune the physical and biochemical properties of a biomaterial by changing the material and/or scaffold architecture. For example, the compressive modulus of poly(caprolactone) (PCL) scaffolds can be significantly increased by printing with higher molecular weight PCL [9]. Scaffold architecture can also be modified to increase scaffold stiffness by decreasing spacing between filaments [10]. In addition, different materials can be printed within the same construct to alter surface chemistry. Di Luca et al. created scaffolds with a gradient in surface hydrophilicity using PCL, poly(lactic acid) (PLA), and a poly(ethylene oxide terephthalate)/poly(butylene terephthalate) (PEOT/PBT) copolymer [11].

Solvent-cast 3D printing (SCP) is a type of direct ink writing that can achieve smaller feature sizes compared to melt-based extrusion techniques like FDM [12–15]. SCP involves dissolving a polymer in a volatile solvent to create an "ink." The ink is extruded from a nozzle, and the solvent rapidly evaporates, leaving behind a solid polymer filament [13,16]. We recently showed that peptide-polymer conjugates can be printed using SCP to produce peptide-functionalized, biodegradable polymer-based scaffolds in a single fabrication step [12,17,18]. Peptide-PCL conjugates were co-dissolved with unmodified high molecular weight PCL (80 kDa), and the peptide emerged on the scaffold surface during solvent evaporation. This modular platform enabled spatial organization of multiple chemistries in a continuous construct. For example, we fabricated scaffolds displaying the canonical cell adhesion peptide RGDS and its negative control RGES on different filaments to spatially control cell adhesion [12]. This strategy was also used to fabricate scaffolds with cartilage-promoting and bone-promoting peptides in discrete regions to mimic the organization of osteochondral tissue [17].

Our prior work showed that introducing peptide-PCL conjugates to the ink did not cause observable changes in scaffold architecture [12,17]. However, adding these lower molecular weight (MW) conjugates (~15-20 kDa) to inks prior to printing may decrease the mechanical properties of the resulting 3D-printed constructs. Polymer MW and MW distribution are known to affect mechanical properties [19,20]. Hendrikson et al. demonstrated a significant decrease in the modulus of 3D-printed PCL scaffolds from 204.2 \pm 8.6 MPa to 146.5 \pm 7.6 MPa when PCL MW was decreased from 65 kDa to 14 kDa, respectively [21]. Dependence between biochemical and physical properties makes it difficult to determine which scaffold property is driving desired cellular responses [22,23]. For example, hydroxyapatite mineral is often integrated into scaffolds as a biochemical cue to drive bone formation, but its addition simultaneously induces an increase in stiffness [24-28]. Since mechanical properties alone are known to influence cell behavior [29], it is difficult to determine whether the presence of hydroxyapatite or change in stiffness contributed to cell response. Strategies to decouple biochemical and physical properties in biomaterials for tissue engineering applications are therefore of great interest. Schoonraad et al. 3D-printed poly(ethylene glycol) diacrylate structures and filled them with biomimetic hydrogels containing extracellular matrix analogs and tethered growth factors [30]. Mechanical properties were tuned by altering the porosity of the 3D-printed structures while the chemical composition of the hydrogels was modified to control stem cell differentiation towards cartilage or bone [30].

The goal of this work was to investigate how different conjugate chemistries and concentrations influence the physical properties of solvent-cast 3D-printed constructs. Here, we compared a positively charged hyaluronic acid-binding peptide-PCL conjugate (HAbind-PCL) and a negatively charged mineralizing peptide-PCL conjugate (E3-PCL) at concentrations ranging from 0 to 18 mg/mL. These amino acid sequences CGGGRYPISRPRKR (HAbind) and CGGGAAAEEE (E3) in these peptide-PCL conjugates were previously used at concentrations of 3 and 18 mg/mL, respectively, to drive human mesenchymal stem cell differentiation towards cartilage and bone for osteochondral tissue

engineering [17]. In this study, the conjugates enabled us to evaluate the effects of peptide sequence, charge, and concentration on conjugate location after printing, architecture, and mechanical properties of solvent-cast 3D-printed filaments and scaffolds. This work demonstrates how our platform combining solvent-cast 3D printing with peptide-polymer conjugates can be used to fabricate 3D-printed constructs with independently tunable biochemical and physical properties.

2. Materials and methods

2.1. Materials

2.1.1. Peptide synthesis and purification

All fluorenylmethyloxycarbonyl choride (Fmoc)-protected amino acids were obtained from AAPPTec (Louisville, KY, USA) except for Fmoc-Lys(N₃)-OH, which was sourced from Chem-Impex International (Wood Dale, IL, USA). Fmoc-Rink-amide 4-methylbenzhydryalmine (MBHA) resin (0.67 mmol/g) and O-benzotriazole-N,N,N',N'-tetramethyluronium-hexafluoro-phosphate (HBTU) were purchased from AAPPTec. Piperidine was purchased from Chem-Impex International. Diisopropylethylamine (DIEA), triisopropylsilane (TIS), and acetonitrile (ACN) were purchased from Sigma-Aldrich (St. Louis, MO, USA), Diethyl ether (DEE), N,N-dimethylformamide (DMF), and dichloromethane (DCM) were purchased from VWR (Radnor, PA, USA). N,N'-diisopropylcarbodiimide (DIC) was purchased from TCI America (Portland, OR, USA). Trifluoroacetic acid (TFA) was purchased from Alfa Aesar (Haverhill, MA, USA). Ethyl (hydroxyimino)cyanoacetate (Oxyma) was purchased from CEM Corporation (Matthews, NC, USA). Dithiothreitol (DTT) was purchased from Gold Biotechnology (Olivette, MO, USA). Ninhydrin test kits were purchased from AnaSpec (Fremont, CA, USA).

2.1.2. Peptide-PCL conjugate synthesis

Anhydrous 1-methyl-2-pyrrolidinone (NMP) was purchased from Alfa Aesar. Dimethyl sulfoxide (DMSO) was purchased from VWR (Radnor, PA, USA). Polycaprolactone (PCL) ($M_{\rm w}$ 14,000 Da), deuterated dichloromethane (CD_2Cl_2), and deuterated dimethyl sulfoxide (DMSO- d_6) were purchased from Sigma-Aldrich. P-Maleimidophenyl isocyanate (PMPI) was purchased from Chem-Impex International.

2.1.3. Solvent-cast 3D printing

Polycaprolactone (M_n 80,000 Da) was generously provided by Polysciences, Inc. (Warrington, PA, USA). 1,1,1,3,3,3,-Hexafluoro-2-propanol (HFIP) was purchased from Matrix Scientific (Elgin, SC, USA).

2.1.4. Peptide labeling

Phosphate buffered saline (PBS) tablets were purchased from Enzo Life Sciences (Farmingdale, NY, USA). Dimethyl sulfoxide (DMSO) and isopropyl alcohol (IPA) were purchased from VWR. Bovine serum albumin (BSA), polyoxyethylenesorbitan monolaurate (TWEEN 20), Triton X-100, sodium azide, and streptavidin-fluorescein isothiocyanate (streptavidin-FITC) were purchased from Sigma-Aldrich. Dibenzocyclooctyne-cyanine3 (DBCO-Cy3) was purchased from Sigma-Aldrich and AAT Bioquest (Pleasanton, CA, USA).

2.1.5. Scaffold sectioning

Optimal Cutting Temperature (OCT) was purchased from Fisher Scientific (Waltham, MA, USA). Chitosan was purchased from Sigma-Aldrich. Acetic acid and Vector Labs ImmEdge $^{\text{TM}}$ Hydrophobic Barrier Pens were purchased from VWR.

2.2. Peptide-PCL conjugate synthesis

Peptides were synthesized and purified using methods previously described [12,17,18,31,32]. Briefly, synthesis was performed using a fluorenylmethyloxycarbonyl chloride (Fmoc)-Rink-Amide 4-methylbenzhydralmine (MBHA) resin (100–200 mesh, 0.67 mmol/g

functionalization) and Fmoc-protected amino acids. CGGGRYPISRPRKR (HAbind), CGGGAAAEEE (E3), and CGGGAAAEEEK(azide) (E3(azide)) peptides were synthesized on a CEM Liberty Blue automated microwave peptide synthesizer (CEM Corporation; Matthews, NC, USA). For CGGGRYPISRPRKRK(biotin) (HAbind(biotin)), Fmoc-Lys(Mtt)-OH was manually coupled to the resin, the Mtt protecting group was removed, and biotin was coupled to the ϵ -amine on the lysine side chain. The remaining amino acids were added using the automated microwave peptide synthesizer. HAbind(biotin) and E3(azide) were used for fluorescent labeling experiments.

Peptides were cleaved from the resin by agitating in a solution of 95 % (v/v) trifluoroacetic acid (TFA), 2.5 % (v/v) ultrapure water, 2.5 %(v/v) triisopropylsilane (TIS), and 2.5 % (w/v) dithiothreitol (DTT). TFA was removed via rotary evaporation, and the remaining liquid was added to a 10-fold volume of cold diethyl ether (DEE). The precipitate was collected by centrifugation and dried under vacuum before purifying using reverse-phase preparative high-performance liquid chromatography (HPLC; Agilent 218 Prep HPLC, Agilent Technologies, Santa Clara, CA, USA) on an Agilent 5 Prep-C18 column (150 mm \times 21.2 mm, 5 μm pore size, 100 Å particle size). The purified peptide was confirmed using electrospray ionization mass spectrometry (ESI-MS; Applied Biosystems 3200 O Trap, Foster City, CA, USA) or matrix assisted laser ionization (MALDI; Shimadzu 8020, Kyoto, Japan) and analytical HPLC on an Agilent 5 Prep-C18 analytical column (150 mm \times 4.6 mm, 5 μm pore size, 100 Å particle size). Additional details and supporting data are provided in the Supplementary (Figs. S1-S4).

Peptide-polycaprolactone (PCL) conjugates (HAbind-PCL, E3-PCL, HAbind(biotin)-PCL, and E3(azide)-PCL) were synthesized using methods previously described [12,17,18,31,32]. Briefly, PCL diol ($M_{\rm W}$ 14,000 Da) was dissolved in anhydrous 1-methyl-2-pyrrolidinone (NMP) under nitrogen. P-Maleimidophenyl isocyanate (PMPI) was dissolved in anhydrous NMP at 20 M equivalents to PCL and added dropwise to the PCL solution while stirring under nitrogen and reacted overnight. The resulting PCL-maleimide (PCL-mal) was precipitated in DEE to remove excess PMPI. PCL-mal was dried under vacuum and stored at $-20\ ^{\circ}\text{C}.$

For each peptide, PCL-mal was dissolved in anhydrous NMP under nitrogen. The peptide was separately dissolved in NMP (HAbind and HAbind(biotin)) or dimethyl sulfoxide (E3 and E3(azide)) at 8 M equivalents to PCL-mal. The peptide solution was added dropwise to the PCL-mal solution while stirring under nitrogen and reacted overnight. Peptide-PCL conjugates were precipitated in DEE and washed in ultrapure water (HAbind and HAbind(biotin)) or 25 % ACN in ultrapure water (E3 and E3(azide)) to remove excess peptide. The conjugates were dried under vacuum and stored at 4 °C. Each synthesis step was confirmed by ¹H nuclear magnetic resonance (¹H NMR; Bruker Ascend™ 400 MHz NMR; Bruker, Billerica, MA, USA). Additional details and supporting data are provided in the Supplementary (Figs. S5-S9).

2.3. Ink preparation

Polycaprolactone (PCL; M_n 80,000 Da) inks were prepared in a syringe by dissolving at 370 mg/mL in 1,1,1,3,3,3-hexafluoro-2-propanol (HFIP). Inks containing peptide-PCL conjugates were prepared by dissolving the conjugate at 3, 6, 12, or 18 mg/mL in HFIP in a syringe before adding 370 mg/mL of unmodified PCL (80 kDa). All inks were agitated at room temperature on a wrist action shaker for 48 h and rested for 24 h at room temperature before use. The resulting sample groups were defined as: PCL, 3-HAbind, 6-HAbind, 12-HAbind, 18-HAbind, 3-E3, 6-E3, 12-E3, 18-E3. For all experiments, N represented the number of inks tested per sample group.

2.4. Rheology

Rheology was performed at room temperature using a Discovery Hybrid Rheometer (DHR; TA Instruments, New Castle, DE, USA) with a modified parallel plate fixture (25 mm diameter top plate, 40 mm diameter bottom plate) [15]. Samples (350 μ L) were extruded directly from the syringe onto the bottom plate, and the top plate was lowered to a trim gap of 600 μ m. Excess ink was removed before lowering the top plate to a geometry gap of 500 μ m. Step stress growth tests were performed on individual inks (N=6-12 inks/sample group) at a shear rate of 8.96 s⁻¹ for 180 s to avoid solvent evaporation effects [15]. Ink viscosity was measured and averaged across the stable stress plateau (Fig. S10) [15].

2.5. Solvent-cast 3D printing

Inks were solvent-cast 3D printed using a 3-axis EV Series Automated Dispensing System (Nordson EFD, Easton Providence, RI, USA) [15]. Syringes were fitted with a 32G blunt-tip needle (100 μm inner diameter) and extruded using an HP3cc Dispensing Tool (Nordson EFD) for 7-fold applied pneumatic pressure. Glass slides were coated with hairspray before printing scaffolds. Scaffolds were printed in orthogonal patterns with a programmed filament spacing of 260 μm (center to center) and a z-spacing of 45 μm between layers. All scaffolds were printed with a print pressure of 70 psi and a print speed of 0.4 mm/s for the first layer and 0.2 mm/s for all subsequent layers.

Scaffolds for architectural characterization were printed as 5 mm \times 5 mm (length x width) and 200 μm (5 layers) thick. Scaffolds for peptide labeling were printed as 5 mm \times 5 mm and 560 μm (14 layers) thick. Scaffolds for compression tests were printed with an offset orthogonal pattern (Fig. S14) as 6 mm \times 6 mm and 1 mm (24 layers) thick. Filaments for tensile testing were printed in arrays of 25 filaments (60 mm in length) spaced 0.5 mm apart (12.5 mm wide total) using a print pressure of 70 psi and a line speed of 0.4 mm/s.

2.6. Filament diameter measurements

Scaffolds were imaged using a Thermo/FEI Scios Focused Ion Beam Scanning Electron Microscope (SEM; Thermo Fisher, Waltham, MA, USA). Scaffolds were mounted on 12-mm aluminum stubs using carbon tape and coated with iridium using a sputter coater (Electron Microscopy Sciences EMS575X, Hatfield, PA, USA) before imaging. SEM images were used to measure filament diameter manually using the open-source program ImageJ (National Institutes of Health, Bethesda, MD USA) (N=3 inks/sample group, 5 scaffolds/ink, 3 images/scaffold, 5 measurements/image). Measurements were taken only with filaments in the same top layer (Fig. S11).

2.7. Characterizing peptide presentation on scaffold surface

Scaffolds were fluorescently labeled to confirm and quantify peptide presentation on the scaffold surface (N = 3-4 inks/sample group, 3 scaffolds/ink). PCL and HAbind(biotin)-PCL scaffolds were labeled with streptavidin-fluorescein isothiocyanate (streptavidin-FITC) and PCL and E3(azide)-PCL scaffolds were labeled with dibenzocyclooctyne-cyanine 3 (DBCO-Cy3) using methods previously described [12,17,18]. For streptavidin-FITC labeling, scaffolds were blocked overnight at room temperature in a solution of phosphate buffered saline (PBS) with 0.5 %(w/v) bovine serum albumin (BSA) and 0.05 % (ν /v) TWEEN 20 (blocking solution A). After blocking, scaffolds were incubated in $0.3\,\mu M$ streptavidin-FITC in blocking solution A for 1 h and washed twice with PBS followed by twice with ultrapure water for 30 min each. Scaffolds were stored in ultrapure water overnight before quantifying fluorescence with a plate reader and imaging. For DBCO-Cy3 labeling, scaffolds were blocked overnight at room temperature in a solution of PBS with 0.2~% (v/v) TWEEN 20 and 0.2~% (v/v) Triton X-100 (blocking solution B). After blocking, scaffolds were washed twice with ultrapure water for 5 min, dried, and incubated in 50 mM DBCO-Cy3 in PBS with 0.5 % (w/ v) BSA for 1 h. Scaffolds were then washed for 10 min each in the following sequence: PBS, ultrapure water, blocking solution B, ultrapure

water, 50 % (v/v) isopropyl alcohol (IPA), 100% (v/v) IPA, 50% (v/v) IPA, and ultrapure water. Scaffolds were stored in ultrapure water overnight before quantifying fluorescence with a plate reader and imaging.

Scaffolds were dried and cut using a 4-mm biopsy punch. Punches were placed in a black 96-well plate and scanned to measure fluorescence intensity on a Tecan Infinite M200 Pro plate reader (Tecan, Männedorf, Switzerland). Excitation and emission wavelengths were 488 nm and 520 nm, respectively, for streptavidin-FITC and 520 nm and 563 nm, respectively, for DBCO-Cy3. Scaffolds were imaged on a Keyence BZ-X810 Fluorescence Microscope (Keyence, Osaka, Japan) using the relevant excitation wavelengths and filters. The same image settings were maintained for all samples.

2.8. Characterizing peptide location in filament bulk

Scaffolds were sectioned and labeled to determine peptide presence in the bulk (N=3-4 inks/sample group, 1 scaffold/ink, 3 cross sections/ scaffold). Scaffolds were cut in half with a Teflon-coated razor, submerged in Optimum Cutting Temperature compound (OCT), and left overnight at 4 °C. Samples were embedded in fresh OCT on a chuck and frozen at -40 °C. Cross sections (30 µm thick) were obtained via cryosectioning on an OTF5000 cryostat (Bright Instruments, Huntingdon, UK). Samples were sectioned onto Cryofilm Type 3C (SECTION-LAB Co. Ltd., Hiroshima, Japan) using methods previously described to firmly mount sections for labeling procedures [33]. Cryofilm was adhered to glass slides using a solution of 1 % (w/v) chitosan in 0.25 % (v/v) acetic acid [34]. Slides were left upright overnight at 4 °C to create a flat and uniform layer of adhesive under the Cryofilm. Once dry, an Immedge Pen was used to create a hydrophobic barrier around each piece of Cryofilm. Samples were submerged in PBS overnight to remove the OCT.

Cross sections were fluorescently labeled using a similar procedure as described in 2.7. For all blocking, labeling, and washing steps, 75 μL of each solution was added to each cross section. Solutions were gently removed by tilting the slide and wicking away excess using a Kimwipe before adding the next solution. Fluorescent images were taken on a Keyence BZ-X810 Fluorescence Microscope (Keyence, Osaka, Japan). Fluorescence intensity was quantified and compared in the inner core and outer core. The inner core included the inner 50 % of the total filament cross-sectional area, while the outer core represented the outer 50 % of the total filament cross-sectional area (Fig. S12). Five filaments per cross section were analyzed using ImageJ (National Institutes of Health, Bethesda, MD USA). Brightfield images were used to determine filaments edges and center. Raw integrated density, which is the sum of the pixel intensity units, was measured on fluorescent images using ImageJ and normalized to the area.

2.9. Mechanical characterization

2.9.1. Filament tensile testing

Filament arrays were mounted on a paper guide (Fig. S13) and removed from the glass slide with ultrapure water (N=3-4 inks/sample group, 1-2 arrays/ink). The mass of each filament array was measured before loading into a Zwick/Roell Tensile Tester (ZwickRoell LP, Kennesaw, GA, USA) with a 100 N load cell at a gauge length of 40 mm. The paper guide was cut prior to tensile tests, which were performed at a crosshead speed of 25 mm/min to a nominal strain of 500 %. Nominal strain ε_N (%) and standard force F (N) were converted to strain ε (mm/mm) and stress σ (MPa), respectively, using Eqs. (1) and (2) [35], where L is the printed filament length (60 mm), ρ is the density of PCL (1.145 mg/mm³) and m is the mass (mg) of the printed array.

$$\varepsilon = \frac{\varepsilon_N}{100} \tag{1}$$

$$\sigma = \frac{FL\rho}{m} \tag{2}$$

The density of the conjugates was considered negligible given their low concentration relative to unmodified PCL in the inks. The elastic modulus was calculated from the slope of the linear region of the stress-strain curve (Fig. S13). Deviation from linearity was considered when the $\rm R^2$ value dropped below 0.995.

2.9.2. Scaffold compressive testing

Scaffolds were analyzed by performing quasistatic compression experiments with a custom instrumented microindenter (N = 3-5 inks/ sample group, 2-4 scaffolds/ink) [36]. The load head was equipped with a rectilinear cantilever beam and a capacitive displacement probe to measure the deflection of the cantilever. Samples were compressed between two rigid plates using a spherical probe to avoid misalignment and ensure that a compressive force was applied without a bending moment or non-uniform contact pressure distribution (Fig. S14). Initially, the load head was lowered until the spherical probe came in contact with the surface of the top plate. This initial contact position was set as the zero point for stage displacement. The load head was lowered at 10 µm/s to a stage displacement of 150 µm and held for 100 s. The stage was then displaced in 50 µm increments at 10 µm/s with 100 s holds at each depth to a maximum stage displacement of 350 µm. The last second of each hold was considered at equilibrium and used to fit a quasistatic linear relationship between force and compression depth (Fig. S14). The slope of this fit was the scaffold stiffness. Scaffold compressive modulus was calculated using Eq. (3), where E^* is the effective modulus (MPa), K_s is the scaffold stiffness (N/mm), t is the scaffold thickness (1 mm), and A is the scaffold cross-sectional area (36

$$E^* = \frac{K_s t}{A} \tag{3}$$

2.10. Statistical analysis

Statistical comparisons between groups were performed using one-way ANOVA tests. Tukey *post-hoc* tests were performed when equal variances were assumed and Dunnett T3 *post-hoc* tests were performed when equal variances were not assumed. All data is presented as mean \pm standard deviation. Values were considered statistically different when the *p*-value was <0.05. Statistical analyses were performed in SPSS (Version 28, IBM, Armonk, NY, USA).

3. Results and discussion

3.1. Printability of conjugate inks

The viscosity of PCL, HAbind-PCL, and E3-PCL inks was measured at a shear rate (8.96 s⁻¹) equivalent to previously determined printing parameters optimized for solvent-cast 3D printing of PCL [15]. There were no significant differences in viscosity between PCL and all HAbind-PCL and E3-PCL concentrations (Fig. 1). We previously showed that inks with statistically similar viscosities can be printed using the same print parameters to achieve the same morphologies and filament diameters [15]. All inks were therefore printed using the same previously determined parameters. Representative SEM images showed similar filament and pore architectures with no statistical differences in filament diameter across any of the sample groups (Fig. 2). A significant difference in viscosity was found between 3-E3 and 18-E3 inks (Fig. 1B), but this did not affect the printed architecture or filament diameter. These results confirmed that the print parameters were suitable for all ink formulations and that conjugate type and concentration did not affect scaffold architecture.

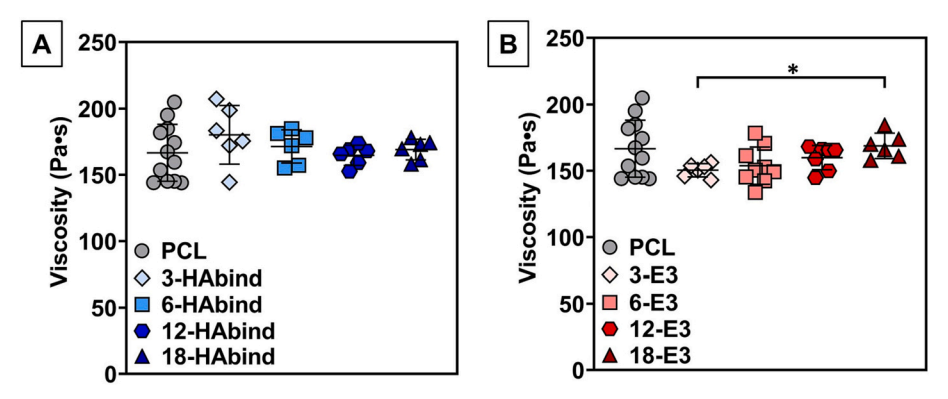


Fig. 1. Viscosity at 8.96 s⁻¹ of inks containing PCL or PCL with (A) HAbind-PCL and (B) E3-PCL conjugate. None of the sample groups were statistically different from PCL. There was a significant difference between 3-E3 and 18-E3 inks. Data is presented as mean \pm SD (*p < 0.05, N = 6–12 inks/group).

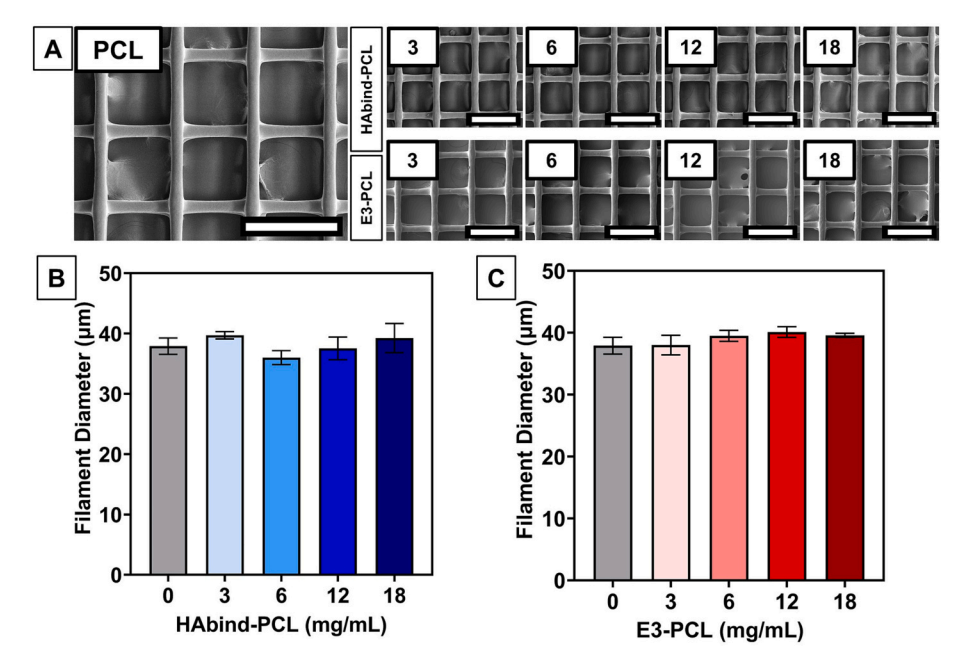


Fig. 2. (A) Representative SEM images of PCL, HAbind-PCL, and E3-PCL scaffolds showing similar filament and pore architectures (scale bar = 300 μ m). Filament diameter was measured from SEM images using ImageJ for (B) HAbind-PCL and (C) E3-PCL scaffolds. Conjugate type and concentration did not significantly affect filament diameter. Data is presented as mean \pm SD (N = 3 inks/group, 4–5 scaffolds/ink, 5 measurements/scaffold).

3.2. Characterizing peptide location on the surface versus in the filament bulk

Biotinylated HAbind-PCL (HAbind(biotin)-PCL) and functionalized E3-PCL (E3(azide)-PCL) conjugates were synthesized to visualize and quantify peptide presentation. Biotin and azide functional groups specifically react with streptavidin [37] and DBCO [38], respectively, through highly efficient click chemistry reactions [39-41]. PCL, HAbind(biotin)-PCL, and E3(azide)-PCL scaffolds were labeled after printing with their respectively tagged fluorophores streptavidin-FITC and DBCO-Cy3 to label peptides available on the surface. Fluorescence imaging and intensity measurements confirmed that the peptides emerged on the surface during solvent-cast 3D printing. Overall, peptide presentation on the surface increased with increasing peptide-PCL conjugate concentration in the ink (Fig. 3). In addition, representative fluorescence images correlated with fluorescence intensity measured using a plate reader. The 3-, 6-, and 12-HAbind(biotin) samples were statistically higher than PCL (Fig. 3A). The 12-HAbind(biotin) scaffolds showed a higher average fluorescence compared to 18-HAbind (biotin) though the difference was not significant (Fig. 3C). Since streptavidin has four binding sites that can react with biotin [42], more than one biotinylated peptides can bind to a single streptavidin. At higher concentrations, binding saturation can therefore occur with fewer streptavidin-FITC molecules, resulting in a lower fluorescence intensity despite a higher concentration of HAbind(biotin) peptides on the surface [43]. For E3(azide)-PCL samples, only 6-E3(azide) was found to have a statistically higher fluorescence compared to PCL (Fig. 3D). However, all concentrations showed fluorescence intensities higher than PCL that increased as expected with increasing E3(azide)-PCL concentration. DBCO has only one binding site that reacts with azide [38], so the surface concentration correlates directly with fluorescence intensity.

Filament cross sections were fluorescently labeled after sectioning the scaffolds, which enabled us to locate peptides within the 3D-printed filament bulk. Notably, conjugate type affected conjugate location within the filament cross-sections. The inner core of the filament showed a similar fluorescence intensity compared to the outer core for all HAbind(biotin) cross-sections (Fig. 4A and C), indicating the conjugate remains within the filament bulk after extrusion and solvent evaporation. For E3(azide)-PCL samples, fluorescence intensity was higher in the outer core closer to the surface compared to the inner core for all

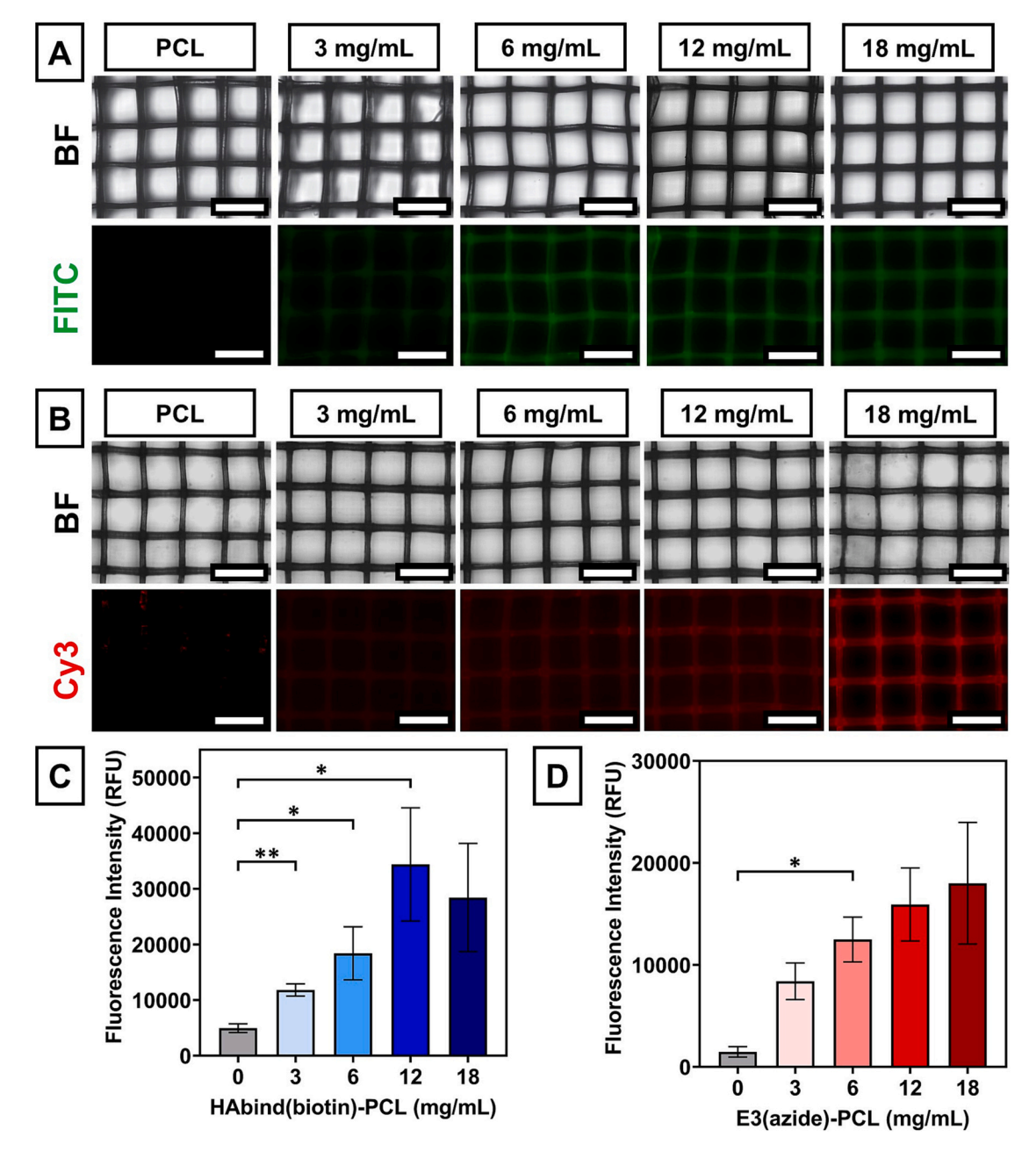


Fig. 3. HAbind(biotin)-PCL and E3(azide)-PCL scaffolds were labeled with streptavidin-FITC (green) and DBCO-Cy3 (red), respectively, to characterize peptide presentation on the scaffold surface. Representative brightfield (BF) and fluorescent images and fluorescence intensity values for (A,C) HAbind(biotin)-PCL and (B,D) E3(azide)-PCL scaffolds (scale bar = $300 \mu m$) showed that peptide presentation on the surface increased with conjugate concentration in the ink. Data is presented as mean \pm SD (*p < 0.05, **p < 0.01, *N = 3–4 inks/group, 3 scaffolds/ink). (For interpretation of the references to colour in this figure legend, the reader is referred to the web version of this article.)

groups (Fig. 4B and D). These results indicated that the negatively charged E3-PCL conjugate migrates more to the surface of the filament compared to the HAbind-PCL conjugate, which largely remains in the filament bulk. In addition, the lower average surface fluorescence seen with 18-HAbind compared to 12-HAbind scaffolds (Fig. 3) may be attributed to HAbind-PCL conjugate being partially trapped within the filament bulk.

Differences in conjugate location between HAbind-PCL and E3-PCL conjugates after solvent-cast 3D printing may be caused by miscibility differences in hexafluoroisopropanol (HFIP). Solvent-cast 3D-printed polymers are dissolved in a solvent with a low boiling point that rapidly evaporates to leave behind a solid polymer filament after extrusion [13,15,16]. Here, HFIP was used as the solvent for all inks.

HFIP is a polar, weakly acidic solvent with a pK_a of 9.3 [44,45]. It has been shown to be a poor nucleophilic solvent, and only weak solvation of cations has been observed [45]. The HAbind (CGGGRYPISRPRKR) peptide contains five basic residues (four arginine (R) and one lysine (K)) with a net positive charge of +5. The E3 (CGGGAAAEEE) peptide includes three acidic residues (three glutamic acids (E)) and has a net negative charge of -3. HAbind-PCL may therefore be less miscible in HFIP compared to E3-PCL and less likely to migrate to the surface with HFIP during solvent evaporation. As a result, more of the HAbind-PCL conjugate would remain in the filament bulk and result in higher fluorescence in the filament core, as shown in Fig. 4A. E3-PCL showed lower fluorescence in the filament bulk compared to HAbind-PCL (Fig. 4B), indicating that higher miscibility in HFIP may drive it to the filament

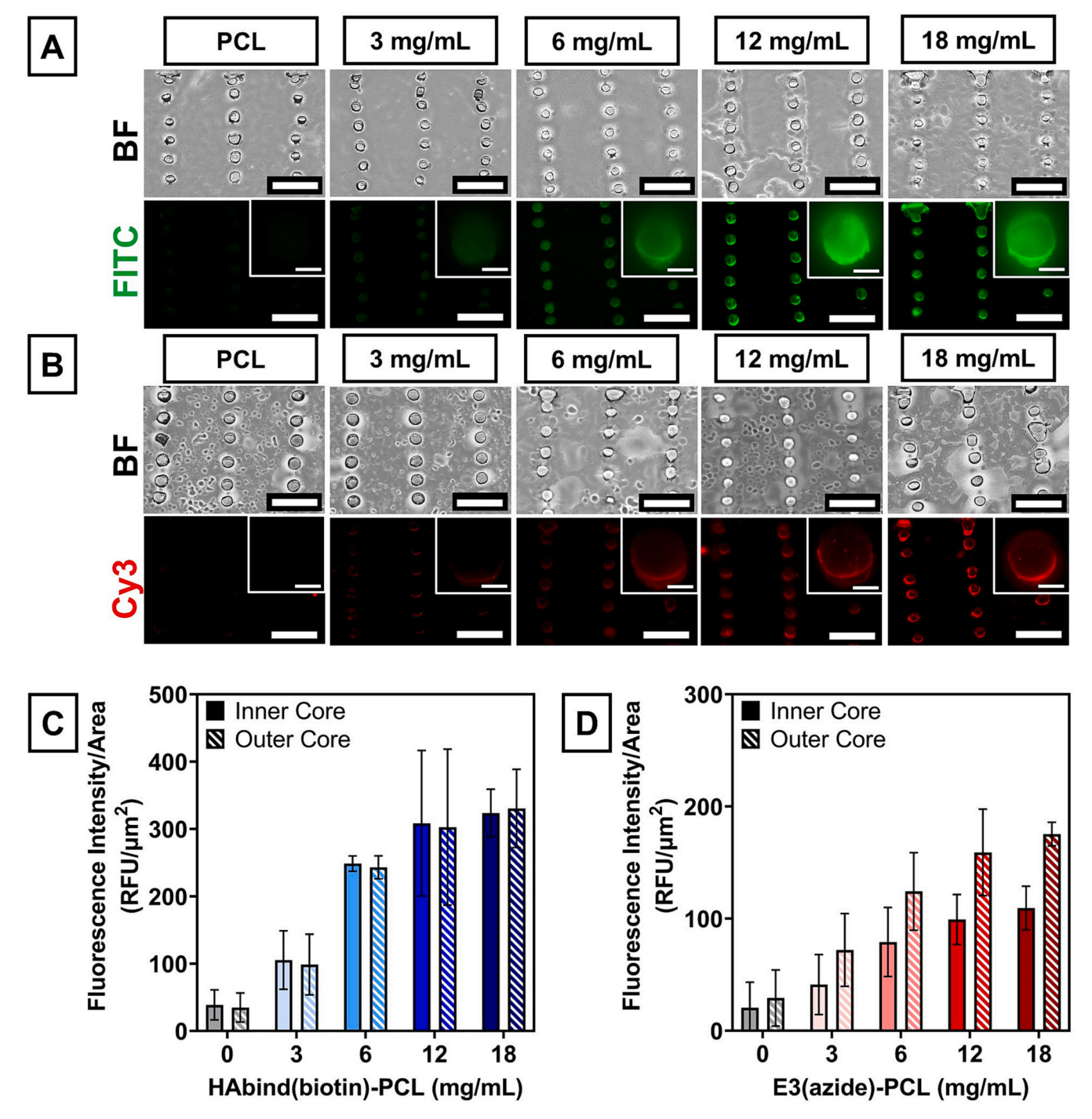


Fig. 4. HAbind(biotin)-PCL and E3(azide)-PCL scaffold cross sections were labeled with streptavidin-FITC (green) and DBCO-Cy3 (red), respectively, to characterize peptide presentation in the filament bulk. Representative brightfield (BF) and fluorescent images were taken for (A) HAbind(biotin)-PCL and (B) E3(azide)-PCL cross sections (scale bar = 200 μ m; inset scale bar = 20 μ m). Fluorescence intensity values were measured in the inner core and outer core for (C) HAbind(biotin)-PCL and (D) E3(azide)-PCL cross sections. Results showed that the HAbind(biotin)-PCL conjugate is presented evenly throughout the filament bulk, while the E3(azide)-PCL conjugate presents more towards the surface. Data is presented as mean \pm SD (N=3 inks/group, 1 scaffold/ink, 3 cross sections/scaffold). (For interpretation of the references to colour in this figure legend, the reader is referred to the web version of this article.)

surface as HFIP evaporates. These differences demonstrate that other solvents could be used to control conjugate location within the filament.

3.3. Influence of peptide-polymer conjugates on mechanical properties

PCL, HAbind-PCL, and E3-PCL filaments and scaffolds were mechanically tested to evaluate how conjugate type and concentration affects mechanical properties. Adding lower MW species have been shown

to decrease mechanical properties [19,20]. Peptide-PCL conjugates (\sim 15–20 kDa) were added at 3, 6, 12, and 18 mg/mL to 370 mg/mL PCL (80 kDa), which respectively correlated to 0.8, 1.6, 3.1, and 4.6 % of the total mass in the ink. These conjugate amounts were relatively low compared to unmodified, high MW PCL content, so conjugate addition was not expected to cause significant changes in mechanical properties. There were no significant differences in tensile modulus between PCL, 3-HAbind, 12-HAbind, and 18-HAbind filaments (Fig. 5A; Table 1) or any

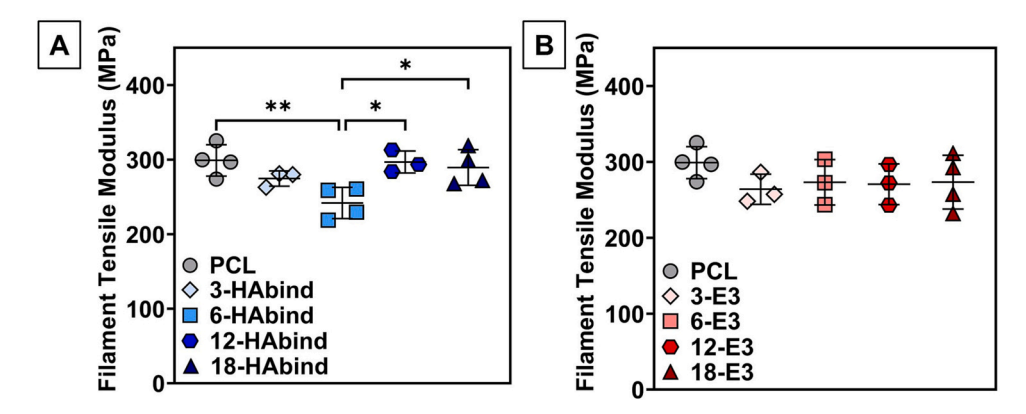


Fig. 5. Tensile modulus of (A) HAbind-PCL and (B) E3-PCL filament arrays. Arrays printed with 6-HAbind inks showed a statistically significantly lower modulus than PCL, 12-HAbind, and 18-HAbind arrays. Data is presented as mean \pm SD (*p < 0.05, **p < 0.01, N = 3–4 inks/group, 1–2 arrays/ink).

Table 1 Filament tensile moduli and scaffold compressive moduli for PCL, HAbind-PCL, and E3-PCL sample groups reported as mean \pm SD.

Sample group	Filament tensile modulus (MPa)	Scaffold compressive modulus (MPa)
PCL	298.94 ± 21.11	0.58 ± 0.06
3-HAbind	274.62 ± 10.32	0.61 ± 0.09
6-HAbind	241.86 ± 20.96	0.47 ± 0.13
12-HAbind	296.75 ± 14.78	0.51 ± 0.04
18-HAbind	289.33 ± 23.91	0.51 ± 0.10
3-E3	263.88 ± 19.97	0.49 ± 0.07
6-E3	273.15 ± 29.94	0.53 ± 0.04
12-E3	270.58 ± 26.78	0.55 ± 0.11
18-E3	273.33 ± 35.43	0.48 ± 0.09

of the E3-PCL sample groups (Fig. 5B; Table 1). HAbind-PCL and E3-PCL conjugates also had no effect on scaffold compressive modulus (Fig. 6; Table 1).

Interestingly, 6-HAbind filaments showed a statistically lower tensile modulus compared to PCL, 12-HAbind, and 18-HAbind sample groups (Fig. 5A; Table 1). There were no significant differences in filament diameter (Fig. 2), indicating this moderate decrease in filament tensile modulus resulted from changes to filament composition. Fluorescence labeling of filament cross-sections showed that the HAbind-PCL conjugate was present in higher concentrations within the filament bulk compared to the E3-PCL conjugate (Fig. 4). The presence of this lower MW conjugate within the filament bulk may disrupt the unmodified, high MW PCL matrix and result in a decrease in filament tensile modulus. Notably, this decrease only occurred with 6-HAbind, an intermediate HAbind-PCL concentration, and higher HAbind-PCL concentrations in 12-HAbind and 18-HAbind filaments did not significantly

impact mechanical properties. The 6-HAbind group may represent a critical concentration where HAbind-PCL conjugates are distributed throughout the PCL matrix and interfere with high MW PCL chain interactions. Representative fluorescence images of the HAbind-PCL cross-sections suggest the HAbind-PCL conjugate accumulates closer to the filament surface with increasing HAbind-PCL concentration (Fig. 4A). The E3-PCL samples further illustrate how conjugate location may impact filament tensile modulus. Fluorescence intensity for E3-PCL samples was consistently higher near the filament surface compared to the bulk across all concentrations (Fig. 4D). The localized E3-PCL concentration near the filament surface may have a lower impact on the unmodified, high MW PCL matrix and filament tensile modulus.

Adding HAbind-PCL or E3-PCL conjugates did not affect scaffold compressive modulus (Fig. 6; Table 1), despite the significant decrease in filament tensile modulus for 6-HAbind samples (Fig. 5; Table 1). Scaffold compressive modulus appeared to decrease with increasing conjugate concentration though no significant differences were found. Filament tensile tests measured the mechanical properties of the material while scaffold compression tests characterized the mechanical properties of the printed architecture. Results suggest that moderate changes in filament tensile properties do not have a significant impact on the scaffold. These differences are likely eclipsed by subtle, random variations in geometry of the printed constructs. There were no significant differences in filament diameter or scaffold architecture (Fig. 2), indicating that scaffold dimensions are more determinant on mechanical properties. This result is not surprising because when the scaffold is under compression, individual filaments deform via bending modes, which are highly sensitive to filament radius. Stiffness of a single simple cantilever beam with a circular cross-section is proportional to radius to the fourth power but is only linearly proportional to elastic modulus.

Overall, the addition of HAbind-PCL and E3-PCL conjugates prior to

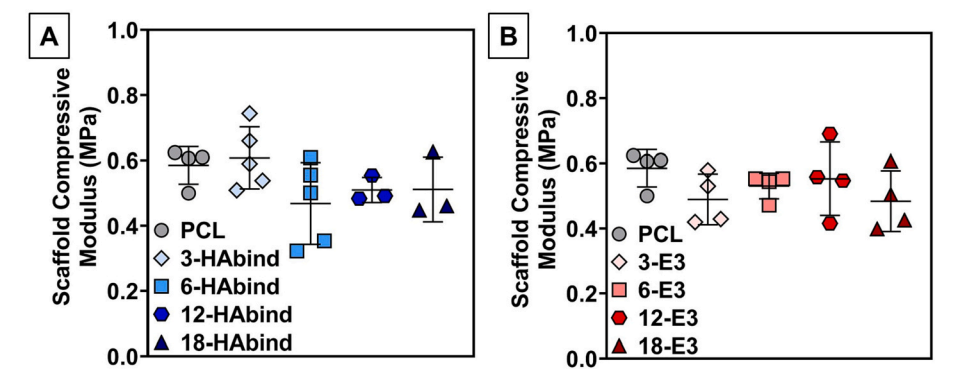


Fig. 6. Compressive modulus of (A) HAbind-PCL and (B) E3-PCL scaffolds. There were no significant differences in scaffold compressive modulus between sample groups. Data is presented as mean \pm SD (N = 3–5 inks/group, 2–4 scaffolds/ink).

solvent-cast 3D printing resulted in peptide-functionalized scaffolds without significantly affecting scaffold architecture or mechanical properties. Others have also focused on developing strategies to modify biochemical and physical properties independently [30,46-50]. For example, hyaluronic acid concentration was increased without altering the mechanical properties of elastin-like protein scaffolds by carefully tuning crosslinker stoichiometry [46]. Others have created hybrid systems that combine mechanically supportive 3D-printed scaffolds with biomimetic hydrogels [30,49,50]. The mechanical properties of the 3Dprinted component can be independently tuned by altering porosity while changing the chemical composition of embedded hydrogels [30]. Here, we demonstrated that our platform combining solvent-cast 3D printing with peptide-polymer conjugates can be used to modify the surface chemistry in a single fabrication step without affecting scaffold architecture or mechanical properties. This strategy to decouple biochemical and physical properties will enable us to fine-tune cellmaterial interactions independently and synergistically.

4. Conclusions

This work demonstrates that peptide-polymer conjugates with different peptide sequences can be added prior to solvent-cast 3D printing to tune biochemical properties without affecting physical properties. Peptide surface concentration was modified by changing ink composition without influencing filament diameter or scaffold architecture. Overall, conjugate type and concentration did not have a significant effect on filament or scaffold mechanical properties. Conjugate chemistry and charge influenced conjugate location within the filament bulk, but these differences did not significantly affect physical properties, even at higher concentrations. We discovered that one intermediate concentration of the positively charged conjugate reduced filament tensile modulus, but this moderate decrease did not affect scaffold compressive modulus. These data illustrate how this versatile platform combining solvent-cast 3D printing with peptide-polymer conjugates can be used to modify surface chemistry and concentration of bioactive cues without significantly changing bulk scaffold properties.

Notably, the significant decrease in filament tensile modulus with one of the conjugate concentrations illustrated how introducing a lower MW species that remains in the filament bulk could be used to intentionally modify mechanical properties. Low and high MW chains of the same polymer can be co-dissolved prior to solvent-cast 3D printing to tune mechanical properties without changing biochemical properties. The downstream potential of this strategy is the ability to generate continuous constructs with independently tunable biochemical and mechanical properties to tightly control desired cell response and tissue regeneration.

CRediT authorship contribution statement

Diana E. Hammerstone: Conceptualization, Formal analysis, Validation, Investigation, Writing – original draft, Project administration, Visualization. Tomas F. Babuska: Methodology, Software, Investigation, Writing – review & editing. Santiago Lazarte: Methodology, Software, Investigation, Writing – original draft. Brandon A. Krick: Conceptualization, Methodology, Resources, Writing – review & editing. Lesley W. Chow: Conceptualization, Methodology, Writing – original draft, Supervision, Funding acquisition.

Declaration of competing interest

The authors declare that they have no known competing financial interests or personal relationships that could have appeared to influence the work reported in this paper.

Data availability

Data will be made available on request.

Acknowledgements

The authors acknowledge Lehigh's Electron Microscopy and Nanofabrication Facility, Institute for Functional Materials and Devices (I-FMD), Health Research Hub (HRH) and Health, Science, and Technology (HST) facilities, and shared instrumentation in the Departments of Biological Sciences and Chemistry. The authors would also like to thank Dr. Hannah L. Dailey for access to the Zwick/Roell Tensile Tester. This work was generously supported by the National Science Foundation (NSF) through a Faculty Early Career Development (CAREER) award (DMR 1944914 to LWC) and Graduate Research Fellowships (DGE 1842164 to DEH; DGE 1842163 to TFB). BAK, TFB, and SL were also supported by NSF CAREER award (CMMI 2027029) to BAK.

Appendix A. Supplementary data

Supplementary data to this article can be found online at https://doi.org/10.1016/j.bioadv.2023.213498.

References

- [1] J.A. Hubbell, Biomaterials in tissue engineering, Bio/Technology. 13 (6) (1995) 565–576, https://doi.org/10.1038/nbt0695-565.
- [2] E.S. Place, N.D. Evans, M.M. Stevens, Complexity in biomaterials for tissue engineering, Nat. Mater. 8 (6) (2009) 457–470, https://doi.org/10.1038/ pp. 104411
- [3] B.S. Kim, C.E. Baez, A. Atala, Biomaterials for tissue engineering, World J. Urol. 18 (1) (2000) 2–9, https://doi.org/10.1007/s003450050002.
- [4] U. Jammalamadaka, K. Tappa, Recent advances in biomaterials for 3D printing and tissue engineering, J. Funct. Biomater. 9 (1) (2018) 22, https://doi.org/10.3390/ jfb9010022.
- [5] G.-H. Wu, S. Hsu, Review: polymeric-based 3D printing for tissue engineering,
 J. Med. Biol. Eng. 35 (3) (2015) 285–292, https://doi.org/10.1007/s40846-015-0038
- [6] M. Guvendiren, J. Molde, R.M.D. Soares, J. Kohn, Designing biomaterials for 3D printing, ACS Biomater. Sci. Eng. 2 (10) (2016) 1679–1693, https://doi.org/10.1021/acsbiomaterials.6b00121.
- [7] N.A. Sears, D.R. Seshadri, P.S. Dhavalikar, E. Cosgriff-Hernandez, A review of three-dimensional printing in tissue engineering, Tissue Eng. Part B Rev. 22 (4) (2016) 298–310. https://doi.org/10.1089/ten.teb.2015.0464.
- [8] N. Poomathi, S. Singh, C. Prakash, et al., 3D printing in tissue engineering: a state of the art review of technologies and biomaterials, Rapid Prototyp. J. 26 (7) (2020) 1313–1334, https://doi.org/10.1108/RPJ-08-2018-0217.
- [9] A.D. Olubamiji, Z. Izadifar, J.L. Si, D.M.L. Cooper, B.F. Eames, D.X.B. Chen, Modulating mechanical behaviour of 3D-printed cartilage-mimetic PCL scaffolds: influence of molecular weight and pore geometry, Biofabrication. 8 (2) (2016), 025020, https://doi.org/10.1088/1758-5090/8/2/025020.
- [10] L. Moroni, J.R. De Wijn, C.A. Van Blitterswijk, 3D fiber-deposited scaffolds for tissue engineering: influence of pores geometry and architecture on dynamic mechanical properties, Biomaterials. 27 (7) (2006) 974–985, https://doi.org/ 10.1016/j.biomaterials.2005.07.023.
- [11] A. Di Luca, A. Longoni, G. Criscenti, et al., Surface energy and stiffness discrete gradients in additive manufactured scaffolds for osteochondral regeneration, Biofabrication. 8 (1) (2016), 015014, https://doi.org/10.1088/1758-5090/8/1/ 015014
- [12] P. Camacho, H. Busari, K.B. Seims, P. Schwarzenberg, H.L. Dailey, L.W. Chow, 3D printing with peptide-polymer conjugates for single-step fabrication of spatially functionalized scaffolds, Biomater Sci. 7 (10) (2019) 4237–4247, https://doi.org/10.1039/c9lmn0887i
- [13] S.Z. Guo, F. Gosselin, N. Guerin, A.M. Lanouette, M.C. Heuzey, D. Therriault, Solvent-cast three-dimensional printing of multifunctional microsystems, Small. 9 (24) (2013) 4118–4122, https://doi.org/10.1002/smll.201300975.
- [14] A. Prasopthum, Z. Deng, I.M. Khan, Z. Yin, B. Guo, J. Yang, Three dimensional printed degradable and conductive polymer scaffolds promote chondrogenic differentiation of chondroprogenitor cells, Biomater. Sci. 8 (15) (2020) 4287–4298, https://doi.org/10.1039/d0bm00621a.
- [15] J.W. Tolbert, D.E. Hammerstone, N. Yuchimiuk, J.E. Seppala, L.W. Chow, Solvent-cast 3D printing of biodegradable polymer scaffolds, Macromol. Mater. Eng. 306 (12) (2021) 2100442, https://doi.org/10.1002/mame.202100442.
- [16] S.Z. Guo, M.C. Heuzey, D. Therriault, Properties of polylactide inks for solvent-cast printing of three-dimensional freeform microstructures, Langmuir. 30 (4) (2014) 1142–1150, https://doi.org/10.1021/la4036425.

- [17] P. Camacho, A. Behre, M. Fainor, K.B. Seims, L.W. Chow, Spatial organization of biochemical cues in 3D-printed scaffolds to guide osteochondral tissue engineering, Biomater. Sci. 9 (20) (2021) 6813–6829, https://doi.org/10.1039/d1bm00859e.
- [18] P. Camacho, M. Fainor, K.B. Seims, J.W. Tolbert, L.W. Chow, Fabricating spatially functionalized 3D-printed scaffolds for osteochondral tissue engineering, J. Biol. Methods 8 (1) (2021), e146, https://doi.org/10.14440/jbm.2021.353.
- [19] R.W. Nunes, J.R. Martin, J.F. Johnson, Influence of molecular weight and molecular weight distribution on mechanical properties of polymers, Polym. Eng. Sci. 22 (4) (1982) 205–228, https://doi.org/10.1002/pen.760220402.
- [20] B.H. Bersted, T.G. Anderson, Influence of molecular weight and molecular weight distribution on the tensile properties of amorphous polymers, J. Appl. Polym. Sci. 39 (3) (1990) 499–514, https://doi.org/10.1002/app.1990.070390302.
- [21] W.J. Hendrikson, J. Rouwkema, C.A. Van Blitterswijk, L. Moroni, Influence of PCL molecular weight on mesenchymal stromal cell differentiation, RSC Adv. 5 (67) (2015) 54510–54516, https://doi.org/10.1039/c5ra08048g.
- [22] X. Wang, T.C. Boire, C. Bronikowski, A.L. Zachman, S.W. Crowder, H.J. Sung, Decoupling polymer properties to elucidate mechanisms governing cell behavior, Tissue Eng. Part B Rev. 18 (5) (2012) 396–404, https://doi.org/10.1089/ten. tels.2012.0011
- [23] S. Jiang, S.C. Li, C. Huang, B.P. Chan, Y. Du, Physical properties of implanted porous bioscaffolds regulate skin repair: focusing on mechanical and structural features, Adv. Healthc. Mater. 7 (6) (2018) 1700894, https://doi.org/10.1002/ adhm.201700894.
- [24] E. Nyberg, A. Rindone, A. Dorafshar, W.L. Grayson, Comparison of 3D-printed poly-e-caprolactone scaffolds functionalized with tricalcium phosphate, hydroxyapatite, bio-oss, or decellularized bone matrix, Tissue Eng. Part A. 23 (11–12) (2017) 503–514, https://doi.org/10.1089/ten.tea.2016.0418.
- [25] H. Qiu, J. Yang, P. Kodali, J. Koh, G.A. Ameer, A citric acid-based hydroxyapatite composite for orthopedic implants, Biomaterials. 27 (34) (2006) 5845–5854, https://doi.org/10.1016/j.biomaterials.2006.07.042.
- [26] J.M. Miszuk, T. Xu, Q. Yao, et al., Functionalization of PCL-3D electrospun nanofibrous scaffolds for improved BMP2-induced bone formation, Appl. Mater. Today 10 (2018) 194–202, https://doi.org/10.1016/j.apmt.2017.12.004.
- [27] N. Sultana, M. Wang, PHBV/PLLA-based composite scaffolds fabricated using an emulsion freezing/freeze-drying technique for bone tissue engineering: surface modification and in vitro biological evaluation, Biofabrication. 4 (1) (2012), 015003, https://doi.org/10.1088/1758-5082/4/1/015003.
- [28] P. Feng, S. Peng, C. Shuai, et al., In situ generation of hydroxyapatite on biopolymer particles for fabrication of bone scaffolds owning bioactivity, ACS Appl. Mater. Interfaces 12 (41) (2020) 46743–46755, https://doi.org/10.1021/ accent lo.13768
- [29] A.J. Engler, S. Sen, H.L. Sweeney, D.E. Discher, Matrix elasticity directs stem cell lineage specification, Cell. 126 (4) (2006) 677–689, https://doi.org/10.1016/j. cell.2006.06.044.
- [30] S.A. Schoonraad, K.M. Fischenich, K.N. Eckstein, et al., Biomimetic and mechanically supportive 3D printed scaffolds for cartilage and osteochondral tissue engineering using photopolymers and digital light processing, Biofabrication. 13 (4) (2021), 044106, https://doi.org/10.1088/1758-5090/ac23ab.
- [31] L.W. Chow, Electrospinning functionalized polymers for use as tissue engineering scaffolds, in: Methods in Molecular Biology vol. 1758, Humana Press Inc., 2018, pp. 27–39. https://doi.org/10.1007/978-1-4939-7741-3-3.
- [32] L.W. Chow, A. Armgarth, J.P. St-Pierre, et al., Peptide-directed spatial organization of biomolecules in dynamic gradient scaffolds, Adv. Healthc. Mater. 3 (9) (2014) 1381–1386, https://doi.org/10.1002/adhm.201400032.
- [33] T. Kawamoto, K. Kawamoto, Preparation of thin frozen sections from nonfixed and undecalcified hard tissues using Kawamoto's film method (2020), in: Methods in Molecular Biology vol. 2230, 2021, pp. 259–281, https://doi.org/10.1007/978-1-0716-1028-2 15. Humana. New York. NY.

- [34] N.A. Dyment, X. Jiang, L. Chen, et al., High-throughput, multi-image cryohistology of mineralized tissues, J. Vis. Exp. 2016 (115) (2016), e54468, https://doi.org/ 10.3701/54468
- [35] A.A. Soufivand, N. Abolfathi, A. Hashemi, S.J. Lee, The effect of 3D printing on the morphological and mechanical properties of polycaprolactone filament and scaffold, Polym. Adv. Technol. 31 (5) (2020) 1038–1046, https://doi.org/ 10.1002/pat.4838.
- [36] B.A. Krick, J.R. Vail, B.N.J. Persson, W.G. Sawyer, Reply to the "discussion of the paper by Krick et al.: Optical in situ micro tribometer for analysis of real contact area for contact mechanics, adhesion, and sliding experiments.", Tribol. Lett. 46 (2) (2012) 207–209, https://doi.org/10.1007/s11249-012-9931-x.
- [37] E.P. Diamandis, T.K. Christopoulos, The biotin-(strept)avidin system: principles and applications in biotechnology, Clin. Chem. 37 (5) (1991) 625–636, https://doi. org/10.1093/clinchem/37.5.625.
- [38] M.R. Karver, R. Weissleder, S.A. Hilderbrand, Bioorthogonal reaction pairs enable simultaneous, selective, multi-target imaging, Angew Chemie. 124 (4) (2012) 944–946, https://doi.org/10.1002/ange.201104389.
- [39] J.E. Moses, A.D. Moorhouse, The growing applications of click chemistry, Chem. Soc. Rev. 36 (8) (2007) 1249–1262, https://doi.org/10.1039/b613014n.
- [40] E.M. Sletten, C.R. Bertozzi, Bioorthogonal chemistry: fishing for selectivity in a sea of functionality, Angew. Chem. Int. Ed. 48 (38) (2009) 6974–6998, https://doi. org/10.1002/anie.200900942.
- [41] R.E. Bird, S.A. Lemmel, X. Yu, Q.A. Zhou, Bioorthogonal chemistry and its applications, Bioconjug. Chem. 32 (12) (2021) 2457–2479, https://doi.org/ 10.1021/acs.bioconjchem.1c00461.
- [42] S. Freitag, I.L.E. Trong, L. Klumb, P.S. Stayton, R.E. Stenkamp, Structural studies of the streptavidin binding loop, Protein Sci. 6 (6) (1997) 1157–1166, https://doi. org/10.1002/pro.5560060604.
- [43] K. Kuningas, T. Rantanen, T. Ukonaho, T. Lövgren, T. Soukka, Homogeneous assay technology based on upconverting phosphors, Anal. Chem. 77 (22) (2005) 7348–7355. https://doi.org/10.1021/ac0510944.
- [44] I. Colomer, A.E.R. Chamberlain, M.B. Haughey, T.J. Donohoe, Hexafluoroisopropanol as a highly versatile solvent, Nat. Rev. Chem. 1 (11) (2017) 1–12, https://doi.org/10.1038/s41570-017-0088.
- [45] B. Carre, J. Devynck, The acidity functions of trifluoroethanol and hexafluoroisopropanol, and their mixtures with water, Anal. Chim. Acta 131(C) (1981) 141–147, https://doi.org/10.1016/S0003-2670(01)93544-5.
- [46] D. Zhu, H. Wang, P. Trinh, S.C. Heilshorn, F. Yang, Elastin-like protein-hyaluronic acid (ELP-HA) hydrogels with decoupled mechanical and biochemical cues for cartilage regeneration, Biomaterials. 127 (2017) 132–140, https://doi.org/ 10.1016/j.biomaterials.2017.02.010.
- [47] K.S. Straley, S.C. Heilshorn, Independent tuning of multiple biomaterial properties using protein engineering, Soft Matter 5 (1) (2009) 114–124, https://doi.org/ 10.1039/b808504h.
- [48] T. Wang, J.H. Lai, L.H. Han, X. Tong, F. Yang, Chondrogenic differentiation of adipose-derived stromal cells in combinatorial hydrogels containing cartilage matrix proteins with decoupled mechanical stiffness, Tissue Eng. Part A. 20 (15–16) (2014) 2131–2139. https://doi.org/10.1089/ten.tea.2013.0531.
- [49] A.C. Daly, D.J. Kelly, Biofabrication of spatially organised tissues by directing the growth of cellular spheroids within 3D printed polymeric microchambers, Biomaterials. 197 (2019) 194–206, https://doi.org/10.1016/j. biomaterials.2018.12.028.
- [50] J.H. Shim, J.Y. Kim, M. Park, J. Park, D.W. Cho, Development of a hybrid scaffold with synthetic biomaterials and hydrogel using solid freeform fabrication technology, Biofabrication. 3 (3) (2011), https://doi.org/10.1088/1758-5082/3/ 3/034102.